ADVANCED FUNCTIONAL MATERIALS
www.afm-journal.de

www.MaterialsViews.com

A Versatile Buffer Layer for Polymer Solar Cells: Rendering Surface Potential by Regulating Dipole

*Wei Zhong, Lie Chen, Shuqin Xiao, Liqiang Huang, and Yiwang Chen**

Spin-coated film of poly(vinylidenefluoride-hexafluoropropylene) (P(VDF-HFP)) acts as a cathode/anode buffer layer in polymer solar cells (PSCs) with conventional/inverted device structures. Such devices show optimized performances comparable with the controlled device, making P(VDF-HFP) a good substitute for LiF/MoO_3 as a cathode/anode buffer layer. Ultraviolet photoelectron spectroscopy (UPS) and Kelvin force microscope (KFM) measurements show that increased surface potential of active layers improves cathode contact. In piezoresponse force microscopy (PFM) measurement, P(VDF-HFP) responds to applied bias in phase curve, showing tunable dipole. This tunable dipole renders surface potential under applied bias. As a result, open-circuit voltage of devices alters instantly with poling voltage. Moreover, positive poling of P(VDF-HFP) together with simultaneous oxidation of Ag gradually improves performance of inverted structure device. Integer charge transfer (ICT) model elucidates improved electrode contacts by dipole tuning, varying surface potential and vacuum level shift. Understanding the function of dipole makes P(VDF-HFP) a promising and versatile buffer layer for PSCs.

1. Introduction

Polymer solar cells (PSCs) are promising candidates for photon-to-electron conversion due to their advantages of lightweight, mechanical flexibility, printing, or roll-to-roll processing at low cost in large sizes.[1,2] In the last decade, a tremendous amount of work has been done to realize the potential of PSCs. Impressive power conversion efficiencies (PCEs) of over 10% have been achieved in a single cell[3] and in tandem solar cells, respectively.[4–6] The understanding of operating principles of PSCs predicted PCE of >20% for a single cell.[7] As 10% efficiency is widely considered to be the threshold to break through into commercial applications, stability and solution processability of PSCs become critical.[8]

In PSCs, electrodes with low/high work functions are desirable to extract electrons/holes and block holes/electrons.[9] Buffer layers called interfacial layers or interlayers are essential for achieving maximum performance in PSCs by tuning interfaces of light-harvesting active layers and charge-collecting electrodes.[10,11] Wide bandgap insulators may better be called surface modifiers,[9,12] when they are employed as buffer layers. In general, energy levels and charge transport properties are considered. Buffer layers are required to collect electrons/holes selectively. Moreover, they can protect active layers from the diffusion of the top electrode,[13] redistribute light intensity within active layers[14,15] or provide an extra internal electrical field.[12]

Solution-processed buffer layers with long-term stability are important for commercial applications. In previous reports, several types of materials have been studied including inorganic metal oxides,[14,16,17] conjugated polymers,[18,19] and nonconjugated polymers.[9,12] Among these materials, non-conjugated polymers are attractive since they have ambient stability and commercial availability. For instance, polyethylenimine ethoxylated (PEIE) can act as a cathode surface modifier,[9] as it is universal to reduce work functions of various electrodes. Poly(vinylidenefluoride-trifluoroethylene) P(VDF-TrFE), a ferroelectric polymer, acts as a good cathode buffer layer (CBL).[12,20] However, there are different views about whether ferroelectricity plays a role in performance improvement. P(VDF-TrFE) films prepared by Langmuir–Blodgett (LB) deposition showed switching polarity of device with poling process.[12] While spin-coated P(VDF-TrFE) films showed no switching character.[20] The differences between these results may have several origins. For example, LB films have much higher crystallinity than spin-coated films.[21] And a high poling field of 200 MV m^{-1} is needed to make P(VDF-TrFE) fully polarized.[22]

In this paper, we focus on spin-coated film of poly(vinylidenefluoride- hexafluoropropylene) P(VDF-HFP) and the function of surface potential controlled by dipole. In piezoresponse force microscopy (PFM) measurement, P(VDF-HFP) responds to applied bias in phase curve, showing tunable dipole. Ultraviolet photoelectron spectroscopy (UPS) and Kelvin force microscope (KFM) measurements confirm that dipole modifies the surface potential of active layers. We use integer charge transfer (ICT) model to understand improved electrode contacts by dipole tuning, variation of surface potential, and vacuum level shift. P(VDF-HFP) serves as a CBL when the dipole increases surface potential, shifting vacuum level to high energy level. After partially polarization to decrease surface potential, P(VDF-HFP) converts to anode buffer layer of inverted PSCs. The PCE of such device increases to 3.1% in

Dr. W. Zhong, Prof. L. Chen, S. Xiao, L. Huang, Prof. Y. Chen
College of Chemistry/Institute of Polymers
Nanchang University
999 Xuefu Avenue, Nanchang 330031, China
E-mail: ywchen@ncu.edu.cn
Dr. W. Zhong
School of Material Science and Engineering
Nanchang Hangkong University
696 Fenghe South Avenue, Nanchang 330063, China

DOI: 10.1002/adfm.201500500

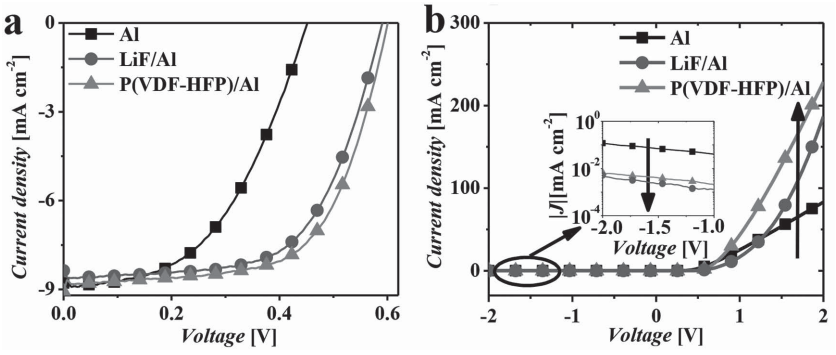

Figure 1. a) *J–V* characteristics of P3HT:$PC_{61}BM$ devices with no cathode buffer (squares), thin layers of LiF (circles), and P(VDF-HFP) (uptriangles) under illumination of an AM 1.5G solar simulator (100 mW cm^{-2}). b) *J–V* characteristics of P3HT:$PC_{61}BM$ devices with no cathode buffer (squares), thin layers of LiF (circles), and P(VDF-HFP) (uptriangles) in the dark. Vertical bars represent the changing direction with buffer layers inserted.

30 d with poling process, which is even higher than the PCE of MoO_3 processed device (3.0% in 30 d). Simultaneous oxidation of Ag and positive poling of P(VDF-HFP) gradually improve device performance. The ferroelectric polymer optimizes device performance for the first time as an anode buffer layer. Understanding the function of dipole makes P(VDF-HFP) a promising and versatile buffer layer for PSCs.

2. Results and Discussion

Figure S1 (Supporting Information) shows chemical structure of P(VDF-HFP). It is employed as a CBL in a conventional device structure of glass/indium tin oxide (ITO)/poly(3,4-ethylenedioxythiophene):poly(styrenesulfonate) (PEDOT:PSS)/poly(3-hexylthiophene) (P3HT): $PC_{61}BM$/P(VDF-HFP)/Al. P(VDF-HFP) solution (1 mg mL^{-1}) is spin-coated on thermally annealed active layers with a thickness of 5 nm (Figure S2, Supporting Information). A reference device without CBL has an average PCE of 1.9%, which is similar to values of 1.64%[23] and 1.98%[24] reported earlier. After insertion of P(VDF-HFP) layer, the PCE distinctly increases to 3.3%, which is even higher than the value of 3.1% obtained from the device with LiF as CBL (**Figure 1**). The effects of P(VDF-HFP) and LiF on devices performance are compared in Figure 1a. It is obvious that P(VDF-HFP) and LiF play the same role of making simultaneous enhancement in open-circuit voltage (V_{oc}) and fill factor (FF). They also reduce the saturated dark current by one order of magnitude, as shown in Figure 1b. In addition, PCEs of devices are in the range of 3.1% to 3.4% with small variations, when P(VDF-HFP) solutions for spin-coating have relatively low concentrations from 2.5×10^{-2} to 1 mg mL^{-1} (**Table 1**). Increasing solution concentration to 2.0 mg mL^{-1} makes FF and V_{oc} decrease slightly with the PCE dropping to 2.9%, due to the insulating nature of P(VDF-HFP). Since solvent treatment takes effect in solar cells based on low-bandgap polymers[25,26] or P3HT,[27,28] the effect of solvent is considered. DMF/methanol (v/v, 1:1) is spin-coated on thermally annealed active layers, and the PCE of corresponding device is 3.3%, almost the same to those of P(VDF-HFP) modified one. As P(VDF-HFP) or solvent treatment here is solution-processed, they are good substitutes for LiF.

To study the surface modifications by solvent and P(VDF-HFP), atomic force microscopy (AFM) measurements are performed; results are shown in **Figure 2**. In AFM topography images, solvent treatment coarsens surface while P(VDF-HFP) makes it smooth. X-ray photoelectron spectroscopy (XPS) spectra do not show chemical modification after solvent or P(VDF-HFP) treatments (Figure S3, Supporting Information). Both treatments increase *C*/*S* ratio of an active layer from 16.7 to 19.3, indicating higher content of $PC_{61}BM$. As 19.3 is still less than calculated value of 23.3, the modified surface is still a P3HT-rich region. Contact angle measurements (Figure S4, Supporting Information) verify XPS results, both solvent treatment and P(VDF-HFP) increase contact angles of water and *n*-hexadecane.

UPS measurements shed a light on how surface modification improves device performance. In **Figure 3**a, after treatments by solvent and P(VDF-HFP), secondary electron cutoff

Table 1. Summary of characteristics for P3HT:$PC_{61}BM$ BHJ solar cells with treatment of P(VDF-HFP) solutions with different concentrations.

Cathode	V_{OC}[a)] [V]	J_{SC} [mA cm^{-2}]	FF [%]	PCE [%] avg	PCE [%] best
Al	0.46	8.9 ± 0.5	48 ± 1	1.9	2.1
Al/P(VDF-HFP) (2.0 mg mL^{-1})	0.58	8.4 ± 0.2	59 ± 2	2.9	3.0
Al/P(VDF-HFP) (1.0 mg/mL)	0.60	8.6 ± 0.4	62 ± 2	3.3	3.5
Al/P(VDF-HFP) (0.4 mg mL^{-1})	0.60	8.7 ± 0.3	64 ± 2	3.3	3.4
Al/P(VDF-HFP) (0.2 mg mL^{-1})	0.61	8.6 ± 0.2	63 ± 1	3.3	3.3
Al/P(VDF-HFP) (0.1 mg mL^{-1})	0.60	8.4 ± 0.2	61 ± 2	3.1	3.2
Al/P(VDF-HFP) (5.0×10^{-2} mg mL^{-1})	0.60	8.2 ± 0.2	65 ± 1	3.3	3.4
Al/P(VDF-HFP) (2.5×10^{-2} mg mL^{-1})	0.61	8.9 ± 0.1	63 ± 1	3.4	3.5
Al/solvent treatment[b)]	0.60	8.6 ± 0.1	63 ± 1	3.3	3.3

P(VDF-HFP) is dissolved in DMF/methanol (1:1, v/v). [a)]The deviation of open-circuit voltage is less than 0.005V; [b)]DMF/methanol (1:1, v/v) was spin-coated on active layer after thermal annealing.

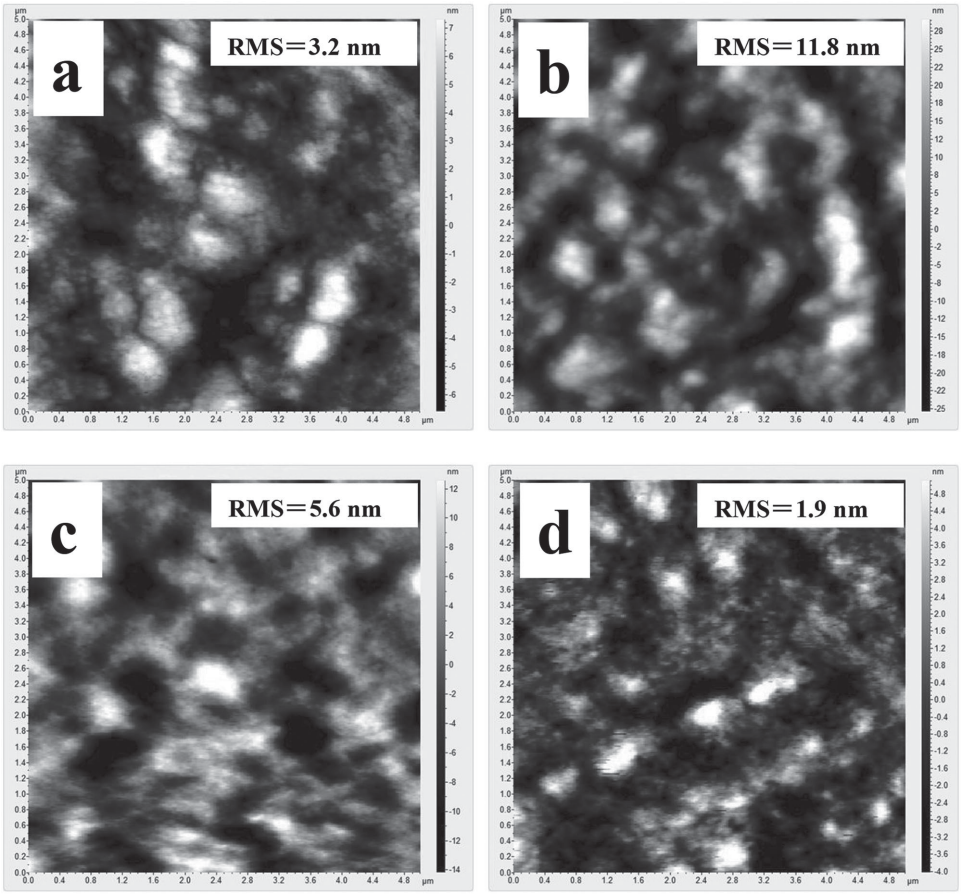

Figure 2. Tapping-mode AFM topography images (5 μm × 5 μm). a) Annealed P3HT: $PC_{61}BM$ blends without treatment. Annealed P3HT:$PC_{61}BM$ blend treated by b) solvent of DMF/methanol (v/v, 1:1), c) P(VDF-HFP) solution with concentrations of 2.5×10^{-2} mg mL^{-1} and d) P(VDF-HFP) solution with concentrations of 1.0 mg mL^{-1}. P(VDF-HFP) was dissolved in DMF/methanol (v/v, 1:1).

(SEC) of active layers move towards the highest occupied molecular orbital (HOMO) onset, with energy offset of 0.30 and 0.55 eV, respectively. Such energy offset means increase of surface potential, which is a common observation for better cathode contacts.[26,29] Figure 3b,c show UPS spectra of pristine P3HT and pristine $PC_{61}BM$, to evaluate the shifted vacuum level of each component. Figure 3d–f are closer views of regions near HOMO onsets of UPS spectra, in which spectrum of P3HT:$PC_{61}BM$ blend resembles that of P3HT. There is thus a P3HT-rich region near the top surface of P3HT:$PC_{61}BM$ blend, in accordance with XPS characterization. **Figure 4** displays a schematic diagram to show the effect of surface dipole Δ on SEC.

ICT model further elucidates the function of surface potential, which explains the principle of energy-level alignments at organic/metal and organic/organic interfaces.[30–32] Before discussion, we must stressed that vacuum level here is the vacuum level at the surface, as describe by Ishii et al.[33] When two solid surfaces come close, their vacuum levels become common. In ICT model, the energy of a positive integer charge-transfer state (E_{ICT+}) and the energy of a negative integer charge-transfer state (E_{ICT-}) are critical to form desirable electrode contacts. When Fermi level of metal is higher/lower than E_{ICT-}/E_{ICT+}, a good cathode/anode contact is promising, with Fermi level pinning to E_{ICT-}/E_{ICT+} in such situations. In the framework of ICT model, the function of P(VDF-HFP) is schematically demonstrated in **Figure 5**. The left part of Figure 5 illustrates the situation without P(VDF-HFP) modification, in which Fermi level of metal is between E_{ICT+} and E_{ICT-}, predicting poor electrode contacts. P(VDF-HFP) brings dipole pointing to inside surface of active layers, increases surface potential, and makes vacuum level of metal shift towards high energy (on the right of Figure 5). The Fermi level of metal is elevated relatively to E_{ICT+}/E_{ICT-} of the semiconductor. As a result, better cathode contact and worse anode contact are forming. ICT model explains why increasing surface potential of active layers improves cathode contacts.

It is clear in UPS measurement that additional dipole after modification increases surface potential and makes better cathode contact. KFM measurements also verify this effect. **Figure 6**a is the surface potential image of annealed active layers. Figure 6b,c are surface potential images of surfaces treated by solvent and P(VDF-HFP), in which surface potential increases by 0.16 and 0.22 V, respectively. UPS and KFM results also show that P(VDF-HFP) increases surface potential more than solvent treatment does (Figure 3a and Figure 6). Capacitance (C)–voltage (V) measurements (Figure S5, Supporting Information) confirm it. For PSC with solvent treatment, the

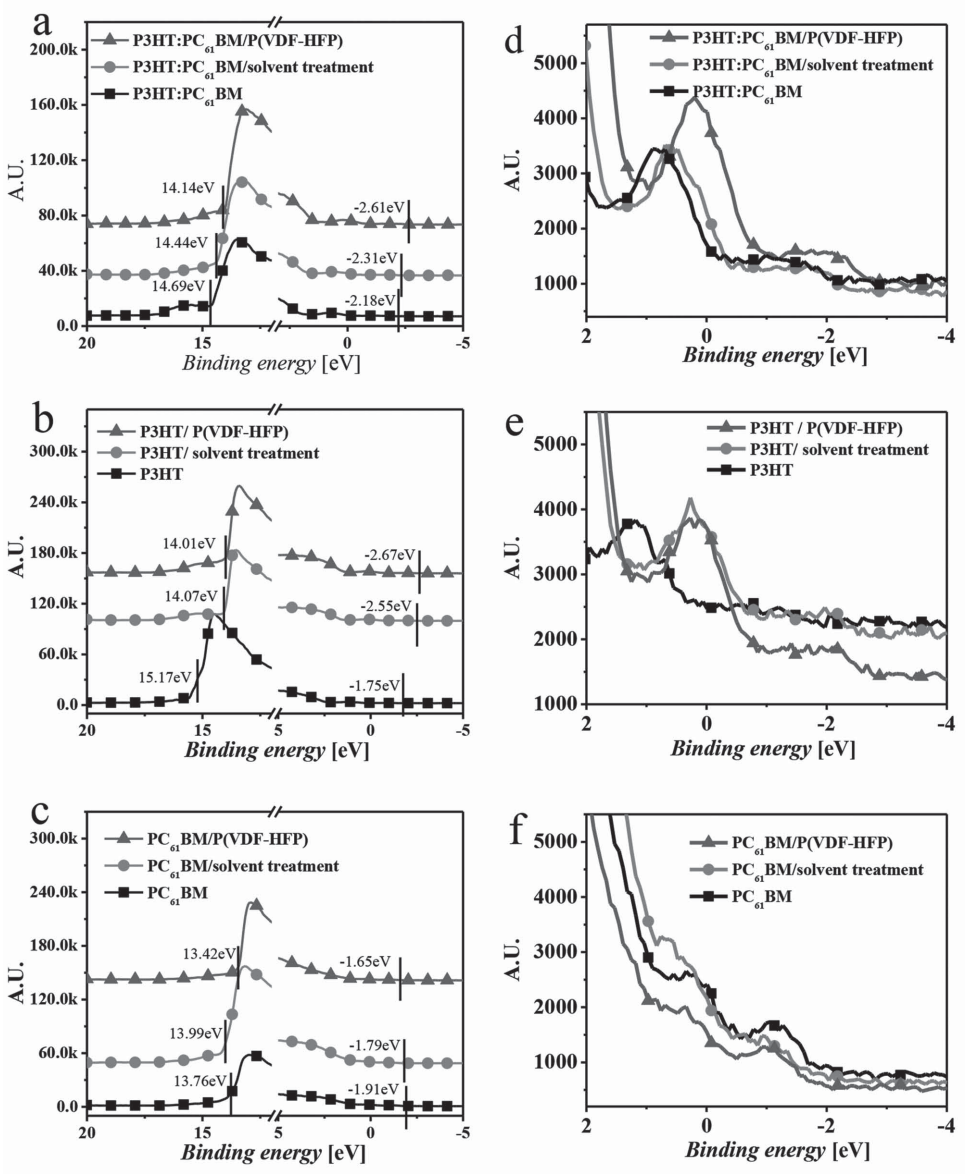

Figure 3. UPS measurements of a,d) P3HT:$PC_{61}BM$ films, b,e) P3HT films, and c,f) $PC_{61}BM$ films, d–f) Closer views of regions near HOMO onsets. The black vertical bars are guides for eyes. Solvent treatment uses DMF/methanol (v/v, 1:1). P(VDF-HFP) was dissolved in DMF/methanol (v/v, 1:1) to prepare a solution with concentration of 1.0 mg mL^{-1}. This solution was spin-coated on P3HT: $PC_{61}BM$ films, P3HT films, and $PC_{61}BM$ films, respectively.

flatband potential is 0.70 V, which increases to 0.81 V in PSC with P(VDF-HFP) buffer layer, indicating a higher surface potential of P(VDF-HFP) spin-coated surface. Although P(VDF-HFP) increases surface potential more than solvent treatment, the resultant device performance is almost the same. ICT model helps to understand this result. If Fermi level of metal is already higher than E_{ICT-} and a good cathode contact is formed, further rendering of metal Fermi level to higher energy just pins Fermi level to E_{ICT-} in such situations.

In previous discussions, increasing surface potential clearly correlates with improved cathode contacts. As P(VDF-HFP) is a ferroelectric polymer, it may respond to electric field and change surface potential to render electrode contact. Stable device with inverted structure of ITO/ZnO/P3HT:$PC_{61}BM$/P(VDF-HFP)/Ag is used to demonstrate whether P(VDF-HFP) can act as an anode buffer layer. However, depolarization of P(VDF-HFP) should be considered, especially when ferroelectric films do not get sufficient compensating charges from semiconductors.[34] In Figure S6, a +10 V voltage for positive poling of devices can produce considerable current density of 4.1 mA cm^{-2}. Thus, there is no problem to compensate polarized P(VDF-HFP). To characterize ferroelectricity film, PFM measurement is usually performed.[35] **Figure 7** shows results of ferroelectric nature of the spin-coated P(VDF-HFP) film by inducing polarization reversal using electrically biased PFM tip. The spin-coated P(VDF-HFP) film shows barely no PFM response in amplitude curve (Figure 7a). Grazing incidence X-ray diffraction (GIXRD)

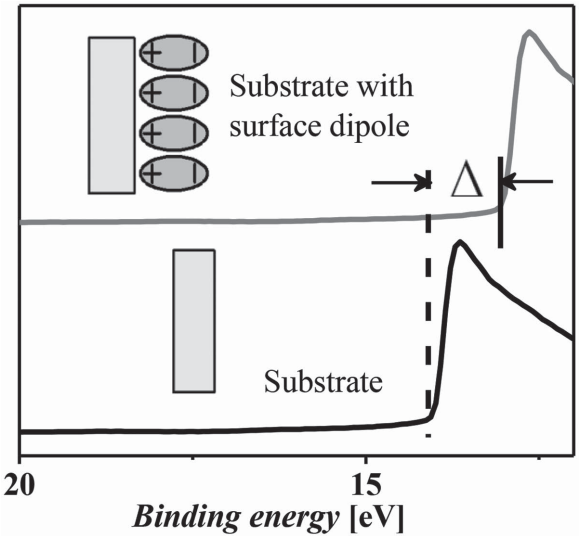

Figure 4. Schematic diagram showing the effect of surface dipole Δ on secondary electron cutoff of UPS spectra.

spectrum (Figure S7, Supporting Information) verifies that spin-coated P(VDF-HFP) has a low crystallinity, in accordance with the amplitude response. In another aspect, phase curve of PFM test (Figure 7b) shows some response. The phase angle increase from –67° to –72°, indicating polarization of P(VDF-HFP). The polarization of P(VDF-HFP) is further confirmed by work functions and KFM measurements. Two plates of ITO/P(VDF-HFP) are overlapped and fixed by clamp as shown in Figure S8 (Supporting Information). A poling voltage of 6 V provided by portable apparatus makes P(VDF-HFP) partially polarized. After separating two plates, dipole on two ITO substrates has opposite direction. The immediate measurements by scanning Kelvin probe show that work function of two substrates is higher/lower than that of ITO/P(VDF-HFP) without poling process (Figure S8, Supporting Information). In another word, poling process can change surface potential of P(VDF-HFP)-coated surface. KFM measurements provide "real-time" effect of dipole on surface potential. Samples with configuration of ITO/ZnO/P3HT:$PC_{61}BM$/P(VDF-HFP) are used. 0, +8, and –8 V DC bias are applied to ITO of sample, the resultant potential images

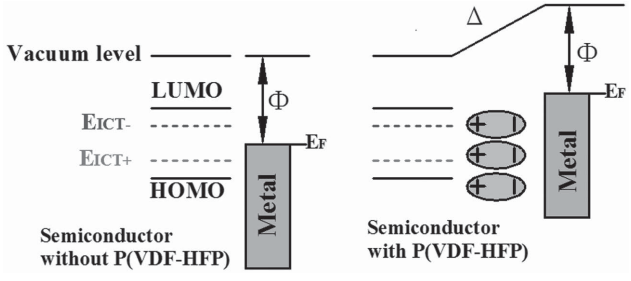

Figure 5. Schematic illustration of the function of dipole brought by P(VDF-HFP). The vacuum levels of metal and semiconductor align before contact when no dipole exists. The vacuum level shifts towards high energy, when the surface dipole points inside of the semiconductor surface to increase surface potential of active layers.

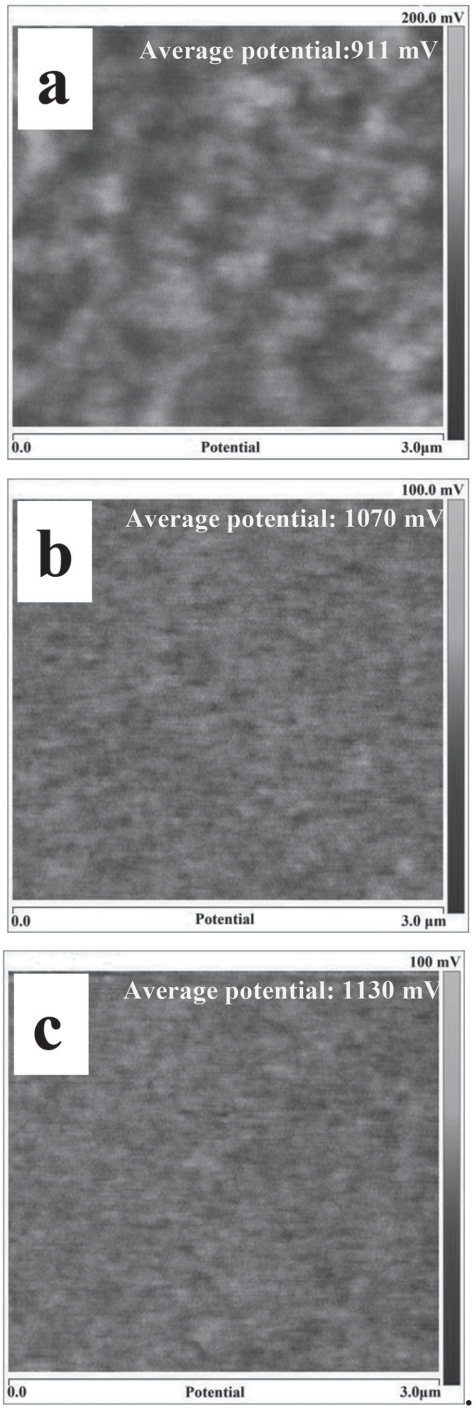

Figure 6. Tapping-mode KFM potential images (3 μm × 3 μm). a) Annealed P3HT:$PC_{61}BM$ blends without treatment. Annealed P3HT:$PC_{61}BM$ blend treated by b) solvent of DMF/methanol (v/v, 1:1), c) P(VDF-HFP) solution with concentrations of 1.0 mg mL^{-1}.

are shown in **Figure 8**a–c. The surface potentials under three conditions are 2.65, 9.77, and –5.08 V. After subtracting DC bias applied to ITO, the surface potential of P(VDF-HFP)-modified surface is 2.65, 1.77, and 2.92 V. +8 V/–8 V bias on ITO makes surface potential decrease/increase by 0.88 V/0.27 V.

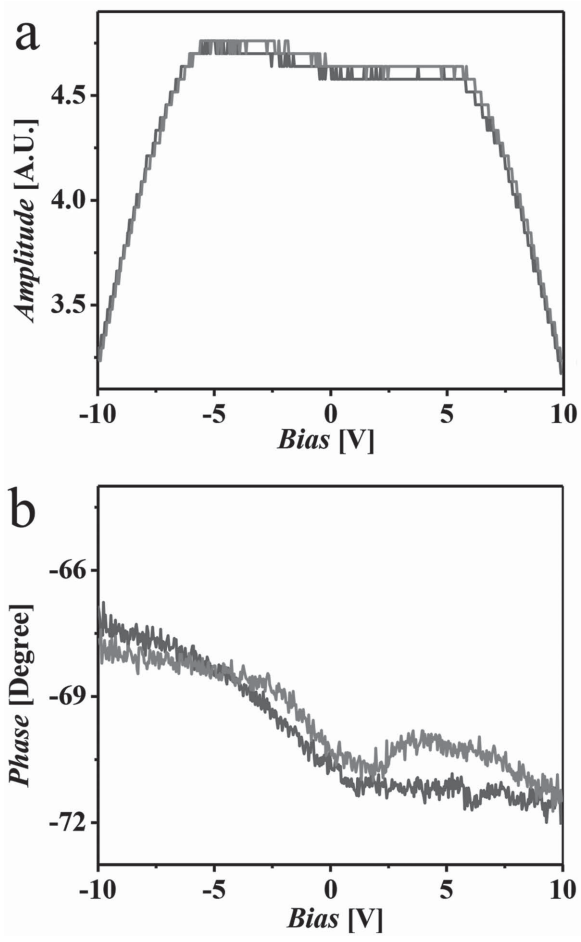

Figure 7. PFM measurements of P(VDF-HFP) on P3HT:$PC_{61}BM$ layer a) amplitude curve under bias loop from –10 V to +10 V b) phase curve under bias loop from –10 V to +10 V.

As P(VDF-HFP) can tune surface potential by poling process, device performance should change with modified electrode contact. For example, the poling process shows an instant effect on V_{oc} as shown in **Figure 9**. Positive poling increases V_{oc} by 0.02 V and negative poling decreases V_{oc} by 0.07 V, in devices with configuration of glass/ITO/ZnO/P3HT:$PC_{61}BM$/P(VDF-HFP)/Ag. To avoid burning thermally evaporated metal, the applied bias for positive poling is set +10 V. The polarizing electric field is about 40 MV m^{-1}, which is lower than reported value of 200 MV m^{-1} to obtain polarization saturation.[22] As a result, device performance improves gradually with time.

The long-term effect of positive poling on performance of devices is studied in inverted devices with configuration of glass/ITO/ZnO/P3HT:$PC_{61}BM$/P(VDF-HFP)/Ag. Reference devices without any anode buffer layer and standard devices with thermally evaporated MoO_3 are prepared for comparison. **Figure 10** shows PCE evolutions of the four devices, where the device with MoO_3 has a constant PCE value of 3.2% in first 20 d. For device without anode buffer layer, the PCE is about 2.1% in first 12 d. The low performance originates from non-selectivity of electrons/holes in anodes. For device incorporated with P(VDF-HFP), initial PCEs are extremely low (below 0.3%), because P(VDF-HFP) forms good cathode contact. In 12 d, the

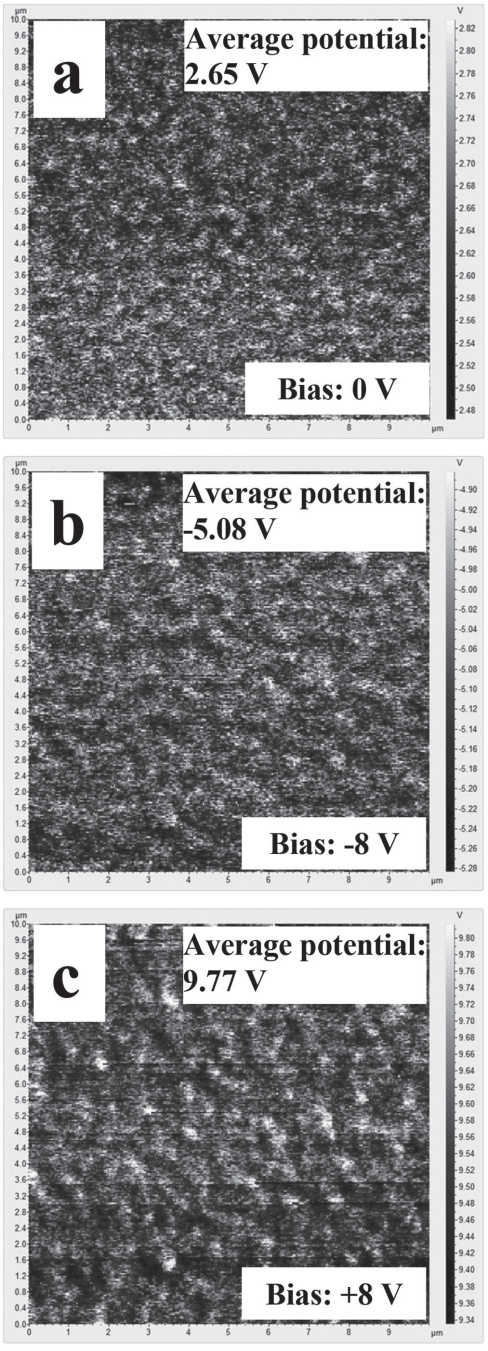

Figure 8. Tapping-mode KFM potential images (10 μm × 10 μm) of P(VDF-HFP)-modified surface. a) Bias of 0 V. b) bias of –8 V c) bias of +8V. Bias is applied to ITO of sample. The sample configuration is ITO/ZnO/P3HT:$PC_{61}BM$/P(VDF-HFP).

PCE of the device with P(VDF-HFP) increase to ≈2.2%, which should originate from a higher work function of anode caused by partially oxidation of Ag.[36] From long term evolution of PCEs of devices, it is evident that P(VDF-HFP) plays the role to make interface stable and offers a tunable dipole to improve anode contacts. The device without anode buffer layer keeps the PCE of 2.1% in 12 d and then drops slowly to 1.7% in 98 d. On the other hand, device with P(VDF-HFP) as an anode buffer

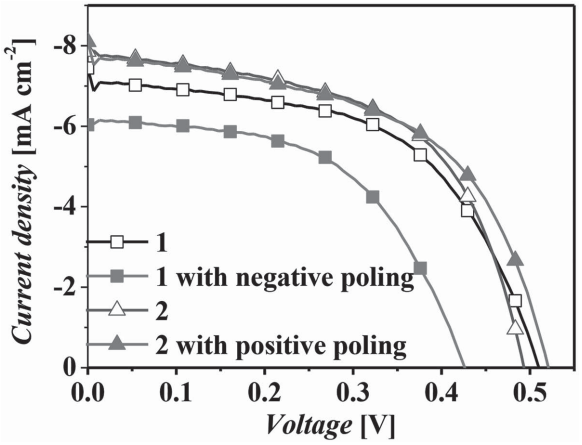

Figure 9. Poling effect on performance of devices, 1 and 2 are two devices stored for 210 d with the same structure of glass/ITO/ZnO/P3HT:$PC_{61}BM$/P(VDF-HFP)/Ag.

layer still has a PCE of 2.2% in 100 d. The effect of Ag oxidation and positive poling is easy to be discriminated. As the device without positive poling shows maximum PCE of 2.2%, while positive poling makes PCE further increase to 3.1% after 30 d, even higher than the PCE of the MoO_3-processed device (3.0% after 30 d). The notably enhanced efficiency is definitely from the modified surface potential brought by tunable dipole to facilitate holes collections. The decreased surface potential makes interface of active layers/metal becomes a worse/better contact of cathode/anode. It is worthy to note that the P(VDF-HFP)-modified devices show good stability, especially for the device undergoes poling process. After 120 d, the PCE of poling device is 2.4%, which is also higher than that of MoO_3-processed device (2.0%). Therefore, tunable dipole make P(VDF-HFP) successful buffer layer for both cathode and anode.

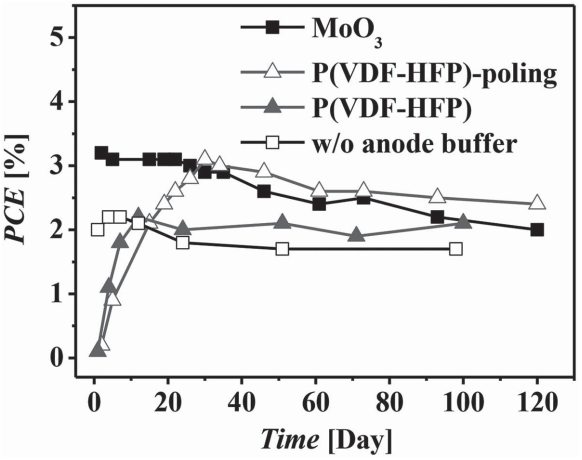

Figure 10. Evolution of PCEs with time in invert device structures, the reference device with invert device structure has a layer sequence of glass/ITO/ZnO/P3HT:$PC_{61}BM$/Ag. The standard device has a layer sequence of glass/ITO/ZnO/P3HT:$PC_{61}BM$/MoO_3/Ag. To study the role of P(VDF-HFP) as anode buffer layer, invert device structure is used with a layer sequence of glass/ITO/ZnO/P3HT:$PC_{61}BM$/P(VDF-HFP)/Ag. The curve with symbol of hollow triangle represents the device employing positive poling.

3. Conclusion

Solution-processed P(VDF-HFP) is demonstrated as buffer layers for conventional and inverted P3HT:$PC_{61}BM$ solar cells. UPS and KFM measurements show that increased surface potential of active layers improves cathode contact. Under applied bias, tunable dipole can alter surface potential and shift vacuum level of active layers, making surface of active layers suitable for cathode or anode contact. As a result, open-circuit voltage of devices alters instantly with poling voltage. Moreover, positive poling of P(VDF-HFP) together with simultaneous oxidation of Ag gradually improves performance of inverted structure device. ICT model elucidates improved electrode contacts by dipole tuning, variation of surface potential, and vacuum level shift. Understanding the function of dipole makes P(VDF-HFP) a promising and versatile buffer layer for PSCs.

4. Experimental Section

Materials: P3HT (M_w = 60–75 kDa, PDI = 1.7–1.9, Rieke Metals Inc.), $PC_{61}BM$ (99.5%, Nano-C), and P (VDF-HFP) (*M*w = 400 kDa; Sigma–Aldrich) were used as received.

Device Fabrication: The conventional device structures are ITO/PEDOT: PSS/P3HT:$PC_{61}BM$/LiF/Al and ITO/PEDOT:PSS/P3HT:$PC_{61}BM$/P(VDF-HFP)/Al. ITO is cleaned by detergent, deionized water, acetone, and isopropanol in an ultrasonic bath in sequence. After exposure to UV light for 20 min, ITO is spin-coated with PEDOT:PSS (Baytron PVP Al 4083) at 4000 rpm for 1 min and annealed in air at 140 °C for 20 min. Films of P3HT:$PC_{61}BM$ are then spin-coated from an *o*-dichlorobenzene (ODCB) solution with P3HT:$PC_{61}BM$ weight ratio of 1:1(P3HT concentration of 20 mg mL^{-1}) at 800 rpm for 30 s. After dried in N_2 glove box, thermal annealing is carried out at 150 °C for 10 min, followed by deposition of 0.8 nm LiF/100 nm Al as cathode (6 mm^2). For devices employing solvent treatment or P(VDF-HFP), DMF/methanol (v/v, 1:1) or P (VDF-HFP) solution of DMF/methanol (v/v, 1:1, 2.5 × 10^{-2} ≈2.0 mg mL^{-1}) is used. Solvent or P (VDF-HFP) solution is spin-coated on thermally annealed active layers at 2000 rpm for 1 min. The surface is thermally annealed at 100 °C for 10 min before final deposition of 100 nm Al. The invert device structures are ITO/ZnO/P3HT:$PC_{61}BM$/MoO_3/Ag and ITO/ZnO/P3HT:$PC_{61}BM$/P(VDF-HFP)/Ag. Sol–gel-derived ZnO films are fabricated using the method reported earlier.[16] Films of P3HT:$PC_{61}BM$ are spin-coated and thermally annealed as in conventional device structures, followed by deposition of 10 nm MoO_3/90 nm Ag or just 90 nm Ag as anode (6 mm^2). For invert devices using P(VDF-HFP) as anode buffer layers, the polymer solution of dimethylformamide (DMF)/methanol (v/v, 1:1, 1.0 mg mL^{-1}) was spin-coated on thermally annealed active layers at 2000 rpm for 1 min. The P(VDF-HFP) film was thermally annealed at 100 °C for 10 min before final deposition of 90 nm Ag. For positive poling of P (VDF-HFP), a +10 V bias is applied to cathode for three times. For negative poling, the applied bias on cathode is −10 V. Devices are short-circuited for 10 times before *I–V* tests are taken. For UPS measurement, an ODCB solution of P3HT:$PC_{61}BM$ (w/w, 1:1, P3HT 5 mg mL^{-1}), P3HT(5 mg mL^{-1}), and $PC_{61}BM$(10 mg mL^{-1}) is used for spin-coating. For other measurements, concentration of P3HT:$PC_{61}BM$ for spin coating is just the same as for device fabrication.

Characterization and Measurement: Current density–voltage (J–V) characteristics of the devices are measured by a Keithley 2400 source meter (Abet Solar Simulator Sun2000), under illumination of an AM

1.5G solar simulator (100 mW cm^{-2}). Silicon reference cell calibrates the light source. Atomic force microscope (Agilent, N9410S) characterizes surface morphology in tapping mode. KFM measurements of unbiased samples and PFM measurements are performed on an atomic force microscope (Multimode V, Veeco) with a diamond-coated tip (DCP11, NT-MDT). KFM measurements of biased samples are performed on N9410S (Agilent) with a Pt-coated tip (DPE14, Micromash). PFM measurements are performed by applying a high-frequency modulating voltage (17 kHz, 7.5 V) to the diamond-coated tip (DCP11, NT-MDT). Amplitude and phase data are acquired in fixed locations of films by applying dc bias superimposed on ac modulation. XPS or UPS measurements are performed on photoelectron spectrometer (ESCALAB 250, Thermo-VG Scientific), with monochromatized Al Kα at 1486.6 eV or He I radiation at 21.2 eV. In UPS measurements, a bias of –8.0 V separates the secondary edges of samples and the analyzer.

Supporting Information

Supporting Information is available from Wiley Online Library or from the author.

Acknowledgements

This work was financially supported by the National Science Fund for Distinguished Young Scholars (51425304), National Natural Science Foundation of China (51273088, 51263016, and 51473075), and National Basic Research Program of China (973 Program 2014CB260409). W.Z. and L.C. contributed equally to this work. The authors thank Prof. Alan J. Heeger, Dr. Huiqiong Zhou, Prof. Nianhua Liu, Prof. Peter Würfel, Dr. M. Oehzelt, and Prof. G. Garcia-Belmonte for stimulating and helpful discussions. The authors also thank Dr. Zhiwen Liu and associated Prof. Zhenghui Liu for KFM and PFM measurements.

Received: February 5, 2015
Revised: March 18, 2015
Published online: April 14, 2015

[1] G. Yu, J. Gao, J. C. Hummelen, F. Wudl, A. J. Heeger, *Science* **1995**, *270*, 1789.
[2] S. Günes, H. Neugebauer, N. S. Sariciftci, *Chem. Rev.* **2007**, *107*, 1324.
[3] Y. Liu, J. Zhao, Z. Li, C. Mu, W. Ma, H. Hu, K. Jiang, H. Lin, H. Ade, H. Yan, *Nat. Commun.* **2014**, *5*, 5293.
[4] J. You, L. Dou, K. Yoshimura, T. Kato, K. Ohya, T. Moriarty, K. Emery, C.-C. Chen, J. Gao, G. Li, Y. Yang, *Nat. Commun.* **2013**, *4*, 1446.
[5] C.-C. Chen, W.-H. Chang, K. Yoshimura, K. Ohya, J. You, J. Gao, Z. Hong, Y. Yang, *Adv. Mater.* **2014**, *26*, 5670.
[6] W. Li, A. Furlan, K. H. Hendriks, M. M. Wienk, R. A. J. Janssen, *J. Am. Chem. Soc.* **2013**, *135*, 5529.
[7] A. J. Heeger, *Adv. Mater.* **2014**, *26*, 10.
[8] M. Jorgensen, K. Norrman, S. A. Gevorgyan, T. Tromholt, B. Andreasen, F. C. Krebs, *Adv. Mater.* **2012**, *24*, 580.
[9] Y. Zhou, C. Fuentes-Hernandez, J. Shim, J. Meyer, A. J. Giordano, H. Li, P. Winget, T. Papadopoulos, H. Cheun, J. Kim, M. Fenoll, A. Dindar, W. Haske, E. Najafabadi, T. M. Khan, H. Sojoudi, S. Barlow, S. Graham, J.-L. Brédas, S. R. Marder, A. Kahn, B. Kippelen, *Science* **2012**, *336*, 327.
[10] H.-L. Yip, A. K. Y. Jen, *Energy Environ. Sci.* **2012**, *5*, 5994.
[11] R. Po, C. Carbonera, A. Bernardi, N. Camaioni, *Energy Environ. Sci.* **2011**, *4*, 285.
[12] Y. Yuan, T. J. Reece, P. Sharma, S. Poddar, S. Ducharme, A. Gruverman, Y. Yang, J. Huang, *Nat. Mater.* **2011**, *10*, 296.
[13] C. J. Brabec, S. E. Shaheen, C. Winder, N. S. Sariciftci, P. Denk, *Appl. Phys. Lett.* **2002**, *80*, 1288.
[14] J. Y. Kim, S. H. Kim, H. H. Lee, K. Lee, W. L. Ma, X. Gong, A. J. Heeger, *Adv. Mater.* **2006**, *18*, 572.
[15] A. K. K. Kyaw, D. H. Wang, D. Wynands, J. Zhang, N. Thuc-Quyen, G. C. Bazan, A. J. Heeger, *Nano Lett.* **2013**, *13*, 3796.
[16] Y. Sun, J. H. Seo, C. J. Takacs, J. Seifter, A. J. Heeger, *Adv. Mater.* **2011**, *23*, 1679.
[17] F. Xie, W. C. H. Choy, C. Wang, X. Li, S. Zhang, J. Hou, *Adv. Mater.* **2013**, *25*, 2051.
[18] Z. He, C. Zhong, S. Su, M. Xu, H. Wu, Y. Cao, *Nat. Photon.* **2012**, *6*, 591.
[19] L. Zhang, C. He, J. Chen, P. Yuan, L. Huang, C. Zhang, W. Cai, Z. Liu, Y. Cao, *Macromolecules* **2010**, *43*, 9771.
[20] K. Asadi, P. de Bruyn, P. W. M. Blom, D. M. de Leeuw, *Appl. Phys. Lett.* **2011**, *98*, 183301.
[21] Y. Yuan, P. Sharma, Z. Xiao, S. Poddar, A. Gruverman, S. Ducharme, J. Huang, *Energy Environ. Sci.* **2012**, *5*, 8558.
[22] S. P. Senanayak, K. S. Narayan, *Adv. Funct. Mater.* **2014**, *24*, 3324.
[23] J.-Y. Jeng, M.-W. Lin, Y.-J. Hsu, T.-C. Wen, T.-F. Guo, *Adv. Energy Mater.* **2011**, *1*, 1192.
[24] Y. Zhao, Z. Xie, C. Qin, Y. Qu, Y. Geng, L. Wang, *Solar Energy Mater. Solar Cells* **2009**, *93*, 604.
[25] S. Li, M. Lei, M. Lv, S. E. Watkins, Z. a. Tan, J. Zhu, J. Hou, X. Chen, Y. Li, *Adv. Energy Mater.* **2013**, *3*, 1569.
[26] H. Zhou, Y. Zhang, J. Seifter, S. D. Collins, C. Luo, G. C. Bazan, N. Thuc-Quyen, A. J. Heeger, *Adv. Mater.* **2013**, *25*, 1646.
[27] H. Li, H. Tang, L. Li, W. Xu, X. Zhao, X. Yang, *J. Mater. Chem.* **2011**, *21*, 6563.
[28] J. H. Jeon, H. K. Lee, D. H. Wang, J. H. Park, O. O. Park, *Solar Energy Mater. Solar Cells* **2012**, *102*, 196.
[29] Z. He, C. Zhong, X. Huang, W.-Y. Wong, H. Wu, L. Chen, S. Su, Y. Cao, *Adv. Mater.* **2011**, *23*, 4636.
[30] S. Braun, W. R. Salaneck, M. Fahlman, *Adv. Mater.* **2009**, *21*, 1450.
[31] H. Wang, P. Amsalem, G. Heimel, I. Salzmann, N. Koch, M. Oehzelt, *Adv. Mater.* **2014**, *26*, 925.
[32] M. Oehzelt, N. Koch, G. Heimel, *Nat. Commun.* **2014**, *5*, 4174.
[33] H. Ishii, K. Sugiyama, E. Ito, K. Seki, *Adv. Mater.* **1999**, *11*, 605.
[34] P. Wurfel, I. P. Batra, *Phys. Rev. B* **1973**, *8*, 5126.
[35] Z. Xiao, Q. Dong, P. Sharma, Y. Yuan, B. Mao, W. Tian, A. Gruverman, J. Huang, *Adv. Energy Mater.* **2013**, *3*, 1581.
[36] M.-Y. Liu, C.-H. Chang, C.-H. Chang, K.-H. Tsai, J.-S. Huang, C.-Y. Chou, I.-J. Wang, P.-S. Wang, C.-Y. Lee, C.-H. Chao, C.-L. Yeh, C.-I. Wu, C.-F. Lin, *Thin Solid Films* **2010**, *518*, 4964.